Applied Catalysis B: Environmental 333 (2023) 122774

Contents lists available at ScienceDirect

Applied Catalysis B: Environmental

journal homepage: www.elsevier.com/locate/apcatb

Superior performance of formaldehyde complete oxidation at ambient temperature over Co single-atom catalysts

Hao Zhang [a], Guanghui Guo [a], Ziyue Wang [a], Qian He [a], Xiaohui He [a,*], Hongbing Ji [a,b,c,**]

[a] Fine Chemical Industry Research Institute, School of Chemistry, Sun Yat-sen University, Guangzhou 510275, China
[b] China Chemistry and Chemical Engineering Guangdong Laboratory, Shantou 515041, China
[c] Advanced Energy Science and Technology Guangdong Laboratory, Huizhou 516000, China

ARTICLE INFO

Keywords:
Formaldehyde removal
High activity
Room temperature
Precursor-atomization strategy
Single-atom catalysts

ABSTRACT

Cost-effective catalysts for the complete oxidation of formaldehyde (HCHO) are essential for indoor air purification and human health. Here, we report a precursor atomization strategy to synthesize cobalt single-atom catalysts (Co SACs), and the Co SACs show complete conversion of 50 ppm HCHO at room temperature and the catalysts are stable during at least 120 h. The HCHO oxidation activity of Co SACs outperforms all the reported non-noble catalysts at room temperature. DFT calculations and isotope experiments reveal the mechanism of HCHO removal over Co SACs that the decomposition of formate intermediates is the kinetically rate-determining step. The excellent formate intermediate decomposition ability of Co SACs is the key factor in achieving excellent HCHO oxidation performance. Considering the facile and versatile SACs synthesis approach, remarkable performance in HCHO abatement, as well as cheap cost, it is believed that this study may open a window for Co SACs industrial application.

1. Introduction

Formaldehyde (HCHO) is one of the major indoor air pollutants and has been classified as a group I carcinogen, which is generally released from building, decorating, and furnishing materials [1,2]. Long-term exposure to HCHO even at ppm level may cause serious adverse effects on human health such as asthma, nausea, eczema, allergy, and vomiting [3]. To effectively eliminate indoor HCHO, various methods have been reported, including physical adsorption [4], photo-assisted oxidation [5], plasma technology [6], and catalytic oxidation [7]. Catalytic oxidation at room temperature is the most desirable and promising technology because it can completely transform HCHO into CO_2 and H_2O over an efficient and stable catalyst, which is favoured as an ideal route for indoor air purification [8,9]. Although supported noble metals (e.g. Pt, Pd, Rh, and Au) have been applied as active components and their activity and stability were proven to meet the demand for indoor formaldehyde abatement at room temperature [10,11], the high price and scarcity of noble metals severely hinder their practical application. The cheap and abundant non-noble metal catalysts are very desirable for the wide demand for the practical HCHO abatement application. Unfortunately, most of the non-noble metal catalysts are primarily composed of single or mixed metal oxides, and their performance of catalytic oxidation of HCHO at room temperature is difficult to meet the requirements of practical applications. For example, the conversion of HCHO on Co_3O_4 at room temperature is only 20.3% [12]. Recently, important progress has been made in the catalytic oxidation of HCHO by non-noble metal catalysts at room temperature. Shen and colleagues [7] reported that Co@NC achieved 88.9% removal of HCHO (100 ppm) at ambient temperature, and Cao et al. [13] found high activity (0.365 $mol_{HCHO}mol_{metal}^{-1}h^{-1}$) and high conversion (97.1%) of MnO_x/AC-N_2 for the catalytic oxidation of HCHO (100 ppm) at room temperature. However, the stability of these catalysts was poor, with Co@NC and MnO_x/AC-N_2 being stable for only 12 h and 4 h, respectively. Our research group has long been focused on developing highly efficient non-noble metal formaldehyde oxidation catalysts. In our previous study, we found that catalyst deactivation was mainly attributed to the accumulation of surface formate intermediates ($HCOO_{ads}$, the intermediate in the HCHO oxidation) [14], which is in good agreement with the recent reports [15–17]. Therefore, development of non-noble metal catalysts with improved decomposition activity of formate intermediates is very beneficial to improve the activity and stability of the catalyst.

* Corresponding author.
** Corresponding author at: Fine Chemical Industry Research Institute, School of Chemistry, Sun Yat-sen University, Guangzhou 510275, China.
E-mail addresses: hexiaohui@mail.sysu.edu.cn (X. He), jihb@mail.sysu.edu.cn (H. Ji).

https://doi.org/10.1016/j.apcatb.2023.122774
Received 17 November 2022; Received in revised form 24 March 2023; Accepted 16 April 2023
Available online 17 April 2023
0926-3373/© 2023 Elsevier B.V. All rights reserved.

Recently, single-atom catalysts (SACs) have received much attention due to their 100% atomic utilization and unique electronic/geometric structure [18]. Many SACs have shown excellent catalytic performance in a range of important reactions, such as selective oxidation [19], selective hydrogenation [20], dehydrogenation [21], hydrogen production [22], various coupling reactions [23–25], and electrochemistry [26–29]. In particular, Beller et al. [30] recently reported that highly dispersed CoN_x species as active sites are the key to excellent formic acid decomposition performance. Inspired by that, the high activity of Co SACs in decomposing formic acid may also benefit for HCHO removal applications. Therefore, we attempt to prepare Co SACs for formaldehyde elimination. Here, we develop a simple, efficient, and versatile method for the synthesis of SACs (termed a precursor atomization strategy) based on the uniform deposition of metal precursor solutions as micro-nano-scale droplets using a home-made atomization device onto the support surface, and then removing the metal ligands by pyrolysis. The Co SACs exhibit highly stable (~120 h) HCHO oxidation performance at room temperature and its high activity (~1.2 $mol_{HCHO}mol_{metal}^{-1}h^{-1}$) outperforms all previously reported non-noble metal catalysts. In-depth studies reveal that the highly dispersed CoN_x active sites favor formate intermediate decomposition and the low HCHO oxidation energy barrier are responsible for the excellent catalytic performance of Co_1/N-C for HCHO oxidation.

2. Experimental section

2.1. Materials

All the solvents and chemicals were available from suppliers and used as received unless specially stated, including tetraamminepalladium(II) nitrate ($H_{12}N_6O_6Pd$, Macklin, 98%), cobalt nitrate hexahydrate ($Co(NO_3)_2{\cdot}6\ H_2O$, Aladdin, 99%), tetraammineplatinum(II) nitrate ($H_{12}N_6O_6Pt$, Alfa Aesar, 99.9%), ferric oxide (Fe_2O_3, Shanghai Yaotian new material technology co., Ltd, 99%), chloroauricacid ($HAuCl_4$, Energy Chemical, 98%), manganese oxide (Shanghai Yaotian New Material Technology co., Ltd, 99%), titanium oxide (TiO_2, Aladdin, 99%), 2-methylimidazole (Aladdin, 98%), carbon black (Alfa Aesar, 99.9%), zirconium dioxide (ZrO_2, Macklin, 99%), cupric oxide (CuO, Aladdin, 99%), methanol (Greagent, 99.5%), formaldehyde (Adamas, 36–38% in water, ACS), formic acid (Saen Chemical Technology (Shanghai) Co., Ltd, 99%), potassium thiocyanate (KSCN, Aladdin, 99%).

2.2. Catalyst preparation

Co_1/N-C was taken as an example to illustrate the preparation of SACs. First, the supports were prepared as follows: the mixture of 2-methylimidazole (2-MI) and carbon black (weight ratio is 1:1) was milled for 10 h at 400 r/min in a planetary ball mill (CHISHUN, QM3SP2), named 2-MI/C. As shown in Fig. S1, the cobalt nitrate solution (2.5 mmol/L, MeOH as solvent) was deposited on 2-MI/C (5 g) through an atomizer (flow rate ~40 mL/h, Shenzhen ikone technology Co.,Ltd,). The heating plate and infrared lamp (50 W, Royal dutch philips electronics Ltd) quickly remove moisture at ~60 °C to ensure continuous drying of the support. After a cumulative consumption of 0.45 L of Co precursor solution, samples were collected. The cotton, steel plate (Φ30 cm), and plastic dome shield (Φ30 cm) were rinsed and filtered to recover unused Co precursors solution. Washed cotton, steel plate (Φ30 cm) and plastic dome shield (Φ30 cm) and filtered to recover the unused cobalt precursor. Pyrolyzed the collected samples at 600 °C for 2 h under flowing nitrogen gas, Co_1/N-C was obtained.

In brief, the atomized metal precursors were sprayed to and molecularly dispersed on the supports, and with subsequent heat treatment, the precursors were decomposed and the corresponding SCAs were formed. Other catalysts, including Pt_1/CuO, Pt_1/ZrO_2, Pd_1/FeO_x, Pd_1/TiO_2, Au_1/FeO_x, Au_1/MnO_x, and Co NPs were prepared by the same synthetic method and the detailed synthetic parameters were shown in Table S1.

2.3. Characterization

Transmission electron microscopy (TEM) and scanning transmission electron microscopy (STEM) images were taken from FEI Tecnai G2 F30 operated at 300 kV. Aberration-corrected high-angle annular dark-field STEM (AC HAADF-STEM) and element mapping were performed over JEM-ARM200F equipped. X-ray absorption spectroscopy (XAS) measurements were conducted on Singapore Synchrotron Light Source (SSLS), the samples were measured in a silicon drift detector and the corresponding metal foils and metal oxides were used as reference samples and measured in the transmission mode. X-ray diffraction (XRD) patterns were obtained from a Bruker's D8 ADVANCE powder X-ray diffractometer with Cu Kα radiation (λ = 1.5418 Å; scanning step= 0.02°). X-ray photoelectron spectrum (XPS) was obtained from ESCA-Lab250 XPS equipped with an Al Kα source and a charge neutralizer. N_2 adsorption-desorption measurements were carried out on a Micromeritic ASAP2020M. Inductively coupled plasma-optical emission spectrometer (ICP-OES) was taken from PerkinElmer OPTIMA 8000DV, and elemental analysis (EA) was measured on the Vario EL cube instrument. In situ diffuse reflectance infrared Fourier transform spectra (DRIFTS) were carried out on a TENSOR 27 spectrometer (Bruker, Germany). The catalyst was pretreated at 120 °C under Ar flow for 1 h. The obtaining background spectra was obtained after the reactor cooled to room temperature. The gas flow was then changed to the reaction gas (150 ppm HCHO, N_2 or 20% O_2 with N_2 balance, GHSV of 12,000 $mL{\cdot}g_{cat}^{-1}{\cdot}h^{-1}$) to record the spectra.

2.4. Catalytic performance test

The catalytic HCHO oxidation activity was evaluated in a fixed-bed reactor. HCHO vapor generated by passing a flow of N_2 through aqueous formaldehyde [4 wt%, bubbled from formalin (36–38% formaldehyde in water), in an ice bath], was diluted by simulated air (25% O_2 with N_2 as balance gas) to get a feed gas composition of ~50 ppm HCHO, relative humidity (RH) ~25%, and 20% O_2 with N_2 as balance gas. The typical flow rate for all the experiments in this article was set at 100 mL/min. The HCHO concentration in the inlet ([HCHO]in) and outlet ([HCHO]out) stream was measured by phenol spectrophotometric method as follows: first, 100 mL of HCHO containing a gas stream was passed through a gas washing bottle loaded with a solution of $C_6H_4SN(CH_3)C{=}NNH_2{\bullet}HCl$ (1×10^{-4} wt%, 5 mL); Then, $NH_4Fe(SO_4)_2{\bullet}12\ H_2O$ (1 wt%, 0.4 mL, dissolved in 0.1 M HCl) was added, and the mixture was left resting in the dark for 15 min. The HCHO concentration was obtained by reading the light absorbance at 630 nm using a spectrophotometer (UV-240, Shimadzu Co., Ltd., Tokyo, Japan) and comparing the data with a standard curve. The standard curve was obtained similarly to the above phenol spectrophotometric method, except for adding a known amount of standard HCHO solution instead of the gas-washing step. The HCHO conversions were calculated based on the changes in HCHO concentrations in the inlet [HCHO]in and outlet [HCHO]out flow:

$$HCHO\quad Conversion(\%) = \frac{[HCHO]_{in} - [HCHO]_{out}}{[HCHO]_{in}} \times 100\%$$

The performance of Co_1/N-C catalytic oxidation of CO was evaluated in a fixed-bed reactor. Feed gas containing 1 vol% O_2, 1 vol% CO, and He (balance) was passed through the reactor (GHSV of 20,000 $mL{\cdot}g_{cat}^{-1}{\cdot}h^{-1}$). The gas composition of the effluent was monitored and analyzed online by a gas chromatograph (GC 7900) equipped.

2.5. KSCN poisoning experiments

The KSCN poisoning experiment was shown as follows: the fresh

Co_1/N-C was added to the KSCN solution (the molar ratio of KSCN to Co was 0.2, 0.4, and 1.5, and denoted as Co_1/N-C 0.2 equiv KSCN, Co_1/N-C 0.4 equiv KSCN, and Co_1/N-C 1.5 equiv KSCN, respectively), stirred for 2 h at room temperature, and then filtered and dried. For the HCHO oxidation test, the reaction conditions were the same as the descriptions in the *2.4 Catalytic Performance Test*. For the FA decomposition test, rates over the catalysts were determined as follows: to a 10 mL solution of 0.05 M FA, 10 mg catalyst was added with reflux and vigorous stirring at 100 °C. The residual FA concentration in the solution was determined by a Shimadzu LC-20 AT HPLC system equipped with a RID-10 A detector and a Bio-Rad Aminex HPX-87 H ion exclusion column (300 ×7.8 mm). The decomposition rate of FA (r) over the catalysts was calculated based on the reaction time and the consumed FA (conversion < 30%).

2.6. Isotopic studies by $^{18}O_2$ pulse method

$^{18}O_2$ isotopic pulse-reaction experiments were performed on a micro fixed-bed reactor connected with an HPR-20 Mass as the detector. 300 mg sample loaded in a quartz tube reactor was first pretreated by helium at 200 °C to remove pre-adsorbed species. After cooling to room temperature, the sample was purged by a flow of gas (12,000 mL·g_{cat}^{-1}·h^{-1}) mixture composed of 150 ppm HCHO, RH ~50% and balance He for 1 h. A successive $^{18}O_2$ pulse was then introduced to the system by operating a six-way valve equipped with a 1 mL sample loop. The $H_2^{18}O$, $C^{16}O_2$, $C^{16}O^{18}O$, and $C^{18}O_2$ in the effluent were recorded by the mass with m/e at 20, 44, 46, and 48, respectively.

2.7. Density functional theory (DFT) calculations

All the calculations were performed by spin-polarized density

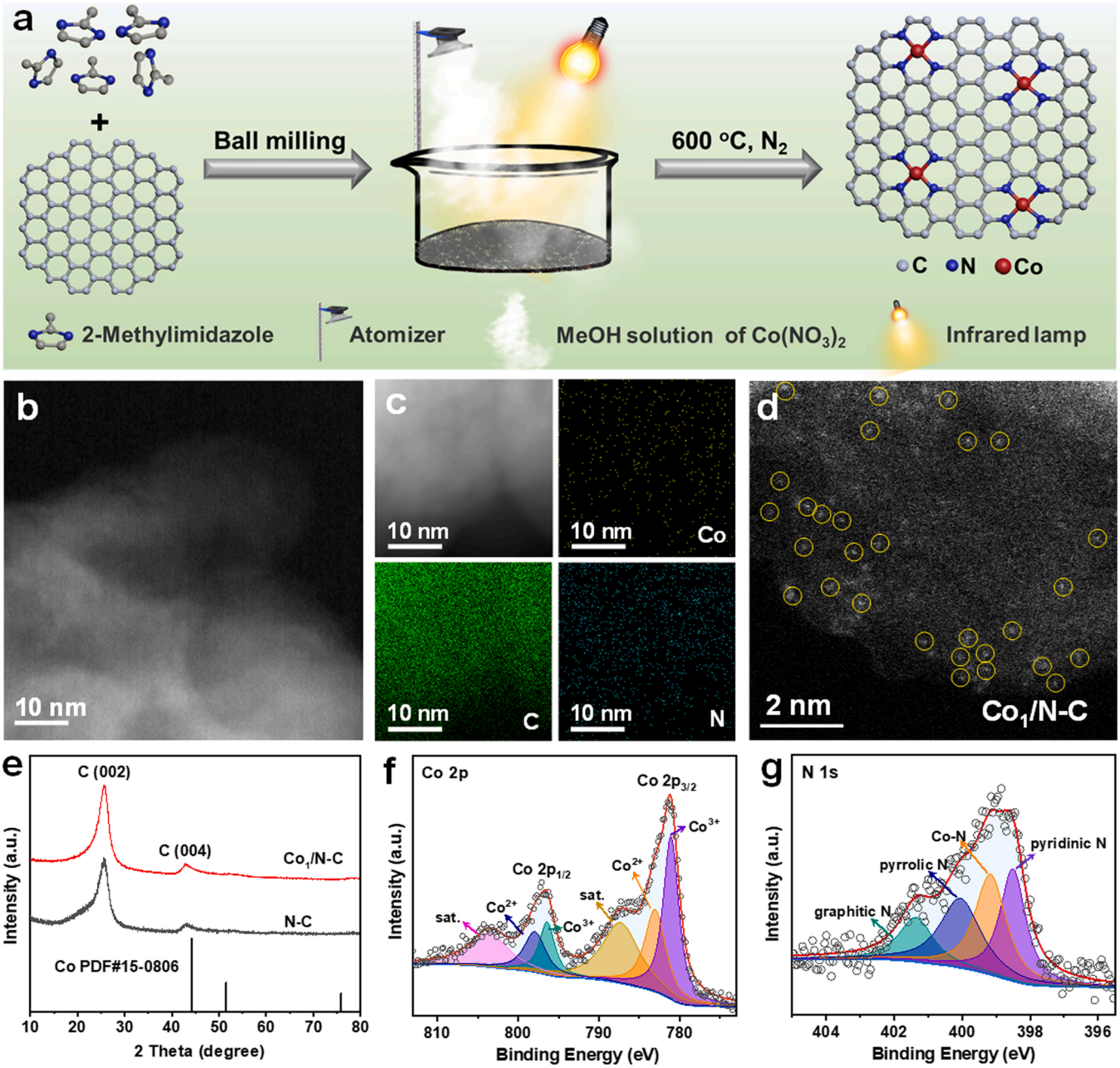

Fig. 1. (a) Schematic diagram of the synthesis of Co_1/N-C. TEM (b), element mapping (c), AC HAADF-STEM images (d), XRD (e), Co 2*p* XPS spectra (f), and N 1 *s* XPS spectra (g) of Co_1/N-C.

functional theory (DFT) as implemented in the Vienna ab initio simulation package (VASP). First-principles calculations were performed based on periodic DFT using the gradient-corrected Perdew-Burke-Ernzerhof functional. The wave functions of valence electrons were composed of the expansion of plane waves with an energy cutoff of 500 Ry. The $2 \times 2 \times 1$ gamma center k-points have been used for geometric optimization. The geometrically optimized consistency tolerances were set to 1.0×10^{-6} eV/atom for total energy and 0.01 eV/Å for force. A large vacuum gap of 15 Å was chosen in the periodically repeated slabs to avoid the interaction between the two surfaces. The climbing image nudged elastic band (CINEB) method was used to locate the transitions of the reaction steps in the HCHO oxidation process. Entropy correction and zero-point energy (ZPE) steps were included in the free energy calculation. The free energy was calculated by the standard formula:

$$\Delta G = E + \Delta ZPE + \Delta H - \Delta TS$$

where ZPE, ΔH, T, and S were the zero-point energy, integrated heat capacity, product temperature, and entropy, respectively.

3. Results and discussion

3.1. Synthesis Co_1/N-C SACs with precursor-atomization strategy

The homemade SACs synthesis equipment was shown in Fig. S1, which was composed of an atomizer (atomized metal precursors), a heating plate and two infrared lamps (ensured supports dryness), a steel plate and a plastic dome shield (formed an enclosed space to facilitate the recovery of unused metal precursors, details see 2.2. Catalyst preparation).

Here we took the synthesis of Co_1/N-C as an example. As shown in Fig. 1a, the fabrication process of Co_1/N-C SACs includes three steps: i) the support (2-MI/C) was obtained by thoroughly mixed 2-MI and carbon black by ball milling method; ii) the dilute solution of the Co precursors was atomized and sprayed onto the support with homemade equipment (Fig. S1); iii) the above sample was heat-treated at 600 °C in N_2 atmosphere to decompose the metal precursors, and the stable Co-N_4 SACs were obtained.

The Co_1/N-C SACs was carefully characterized. The nitrogen contents (~1.65 wt%), specific surface area (~85.3 $m^2 \cdot g^{-1}$), and metal loadings (~0.22 wt%) of Co_1/N-C were listed in Table S2. As expected, the STEM (Fig. 1b) and TEM (Fig. S2) images did not show any observable Co nanoparticles (NPs) due to the highly dispersed Co species in Co_1/N-C. Element mapping analysis of Co_1/N-C (Fig. 1c) indicated that Co and N were homogeneously distributed on the carbon support. No Co NPs peaks (PDF#15–0806) were observed in the XRD patterns of Co_1/N-C (Fig. 1e), further indicating that the Co species were highly dispersed in N-C. The AC HAADF-STEM image (Fig. 1d) for Co_1/N-C showed isolated bright dots corresponding to Co atoms supported on carbon, demonstrating the Co species were atomically dispersed.

The chemical state of surface Co and N species on the catalyst surface was further characterized by XPS. The Co 2*p* XPS spectra of Co_1/N-C in Fig. 1f showed two pairs of peaks ($2p_{3/2}$ and $2p_{1/2}$) at 781.0/796.4 eV and 783.0/797.9 eV assigned to the Co^{3+} and Co^{2+} [7,31]. Deconvolution of N 1 *s* XPS spectra (Fig. 1g) gave pyridinic N (398.5 eV), Co-N (399.2 eV), pyrrolic N (400.0 eV), and graphitic N (401.3 eV), indicating the N atoms were incorporated into the carbon graphite layer as well as the formation of Co-N interaction [32].

XAS measurements were conducted to further confirm the oxidation state and coordination structure of the Co single atoms. X-ray absorption near-edge structure (XANES, Fig. 2a) spectra at Co K-edge showed the energy of Co_1/N-C was located between Co foil and Co_3O_4, indicating that the Co species was at a positive valence state [32], in line with the results of Co 2*p* XPS spectra. The coordination environment of Co species in Co_1/N-C was obtained from the extended X-ray absorption fine structure (EXAFS). The *R* space at about 1.43 Å, estimated from Fourier transformed (FT) k^2-weighted curves at the Co K-edge, was attributed to a single shattering of photoelectrons from Co to nearby N atoms in

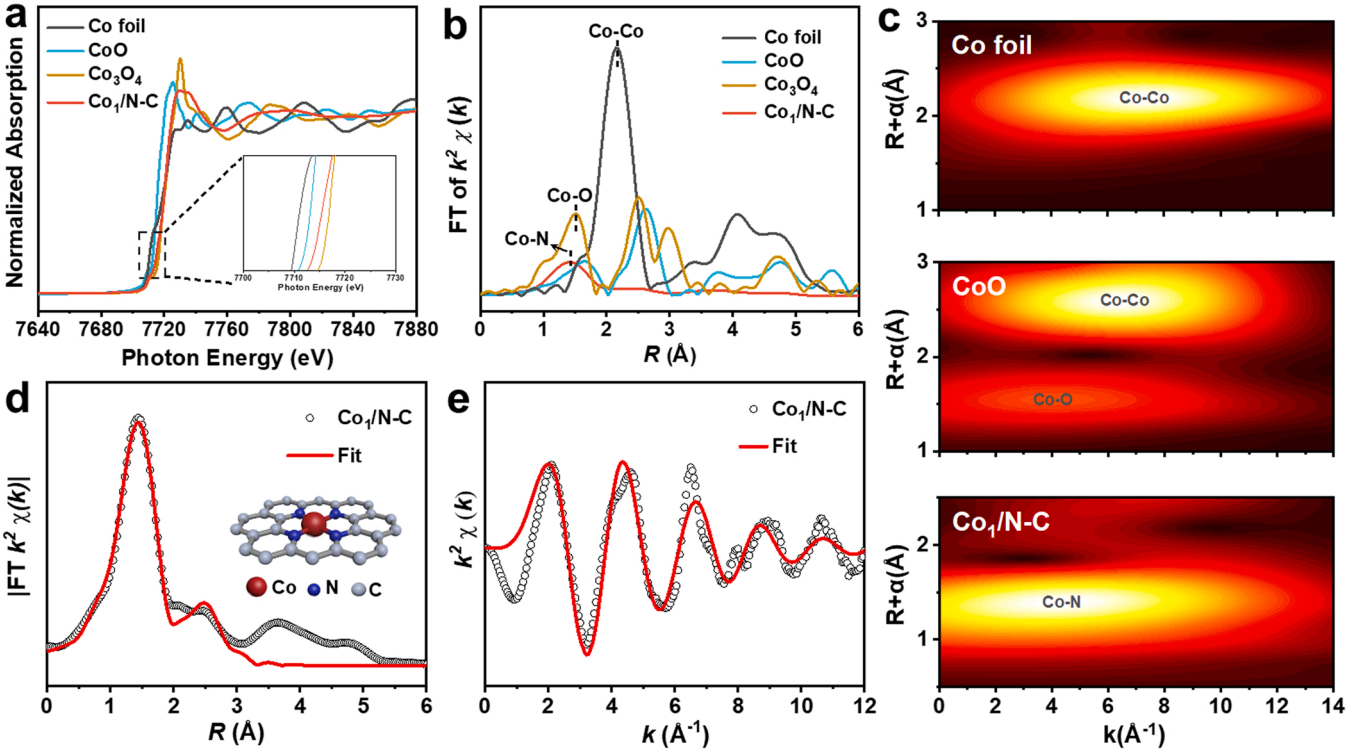

Fig. 2. XANES Co K-edge (a) and EXAFS (b) spectra of Co_1/N-C, CoO, Co_3O_4, and Co foil. (c) WT of Co K-edge EXAFS of Co_1/N-C, CoO, and Co foil. (d) FT k^2-weighted $\chi(k)$-function of the EXAFS spectra for Co K-edge and corresponding R-space fitting curves for the Co_1/N-C. (e) EXAFS *k* space fitting curve and the experimental one of Co_1/N-C.

Co_1/N-C; the feature peak ascribed to Co-Co bond at 2.16 Å was not observed in Co_1/N-C (Fig. 2b) consistent with the results of AC HAADF-STEM [33,34]. Moreover, low *k* values of the lobe (1.43 Å, 4.35 $Å^{-1}$, Co-N) of WT (Fig. 2c) in Co_1/N-C further confirmed the Co–N coordination; a high *k*-value (2.16 Å, 7.50 $Å^{-1}$, Co-Co) of the lobe of wavelet transform (WT, Fig. 2c) was not observed in Co_1/N-C, indicating the central Co was not bound to heavy atoms (e.g., Co), in line with the results of EXAFS [33,34]. The Co-N coordination number determined from the fitting FT-EXAFS of Co_1/N-C (the fitting curve was shown in Fig. 2d-e, and the fitting parameters were collected in Table S3) indicated the Co atoms were coordinated by four neighbouring N bonds.

Surprisingly, the precursor-atomization strategy is remarkably versatile for SACs fabrication. Briefly, the dilute metal precursor solution was deposited on the support by a homemade atomization device and the corresponding SACs were obtained by calcination to remove the metal ligands. Pt_1/CuO, Pt_1/ZrO_2, Pd_1/TiO_2, Pd_1/FeO_x, Au_1/MnO_x, and Au_1/FeO_x were successfully prepared by simply changing the types of metal precursors and supports (details see *2.2. Catalyst preparation* and Table S1). To identify the aggregation states and content of metal species on the supports as well as probe the texture properties of catalysts, all the synthesized SACs were characterized comprehensively by TEM/STEM, element mapping, XRD, ICP-OES, BET, and AC HAADF-STEM (Figs. S3–9 and Tables S2).

3.2. Catalytic performance of Co SACs

The HCHO catalytic oxidation performance of different catalysts was measured with a gas hourly space velocity (GHSV) of 20,000 $mL \cdot g_{cat}^{-1} \cdot h^{-1}$. We used a series of SACs for the formaldehyde oxidation reaction (Fig. S10), the synthesized Co_1/N-C showed the best catalytic performance for formaldehyde oxidation. Co SACs were selected as primary catalysts due to their low cost and high efficiency. As shown in Fig. 3a, Co_1/N-C exhibited complete removal of HCHO. The removal rate of HCHO by Co NPs (~2.1 nm, Fig. S11) and N-C decreased sharply within 1 h, which was attributed to the gradual saturation of adsorption of gaseous HCHO by porous N-C. The catalytic activity of Co_1/N-C (1.183 $mol_{HCHO} mol_{metal}^{-1} h^{-1}$, Fig. 3b) was much higher than that of Co NPs (0.047 $mol_{HCHO} mol_{metal}^{-1} h^{-1}$) and N-C, suggesting the atomically dispersed Co was essential for excellent catalytic activity. Surprisingly, we found that the catalytic activity of Co_1/N-C for formaldehyde oxidation at room temperature, outperformed all the reported non-noble heterogeneous catalysts by at least three times of magnitude (partly because every Co atom contributed directly to the reaction, Fig. 3c, Table S4). In addition, the stability test showed that at room temperature, Co_1/N-C maintained excellent catalytic performance (HCHO conversion >90%, Fig. 3d) within 120 h, which was at the leading edge of what has been reported in the literature (Table S4).

3.3. Catalytic mechanism

There were few studies on the catalytic removal of HCHO by SACs at room temperature, and its catalytic mechanism was still incomplete [2,35]. The catalytic oxidation of HCHO by noble metal SACs at room temperature had recently attracted attention [2], however, the application of non-noble metal SACs was rarely reported. To understand the excellent catalytic performance of Co_1/N-C for HCHO, it was necessary and meaningful to elucidate the catalytic mechanism.

The detection of CO_2 by online mass spectrometry (Fig. 4a) showed that the intensity of the CO_2 signal (m/e=44) on Co_1/N-C strongly depended on O_2 feeding: around its background level under anaerobic

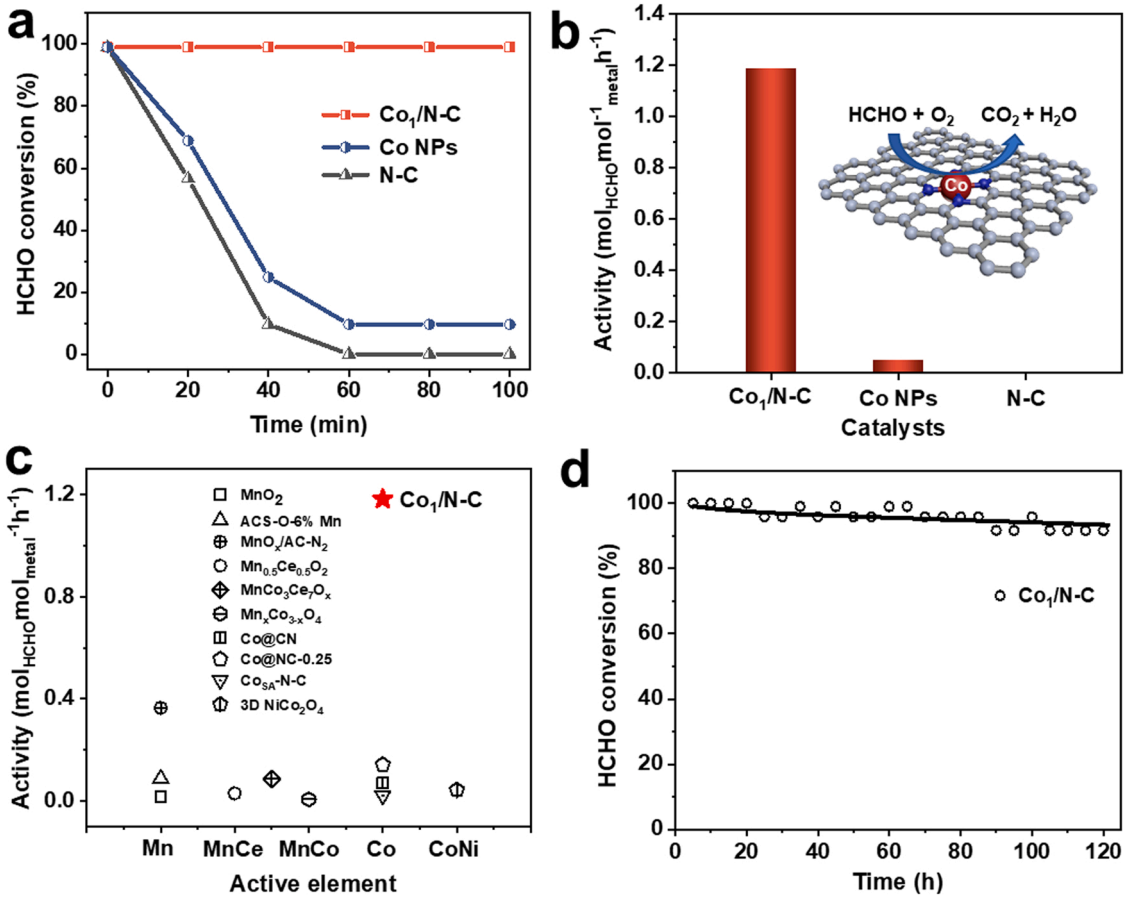

Fig. 3. The HCHO removal rate (a) and catalytic activity (b) of Co_1/N-C, Co NPs, and N-C. (c) Activity comparison of Co_1/N-C with the reported non-noble metal catalysts. (d) Stability test over Co_1/N-C. Reaction conditions: 50 ppm HCHO, 20% O_2, N_2 balance, GHSV of 20,000 $mL \cdot g_{cat}^{-1} \cdot h^{-1}$, RH ~25%, room temperature.

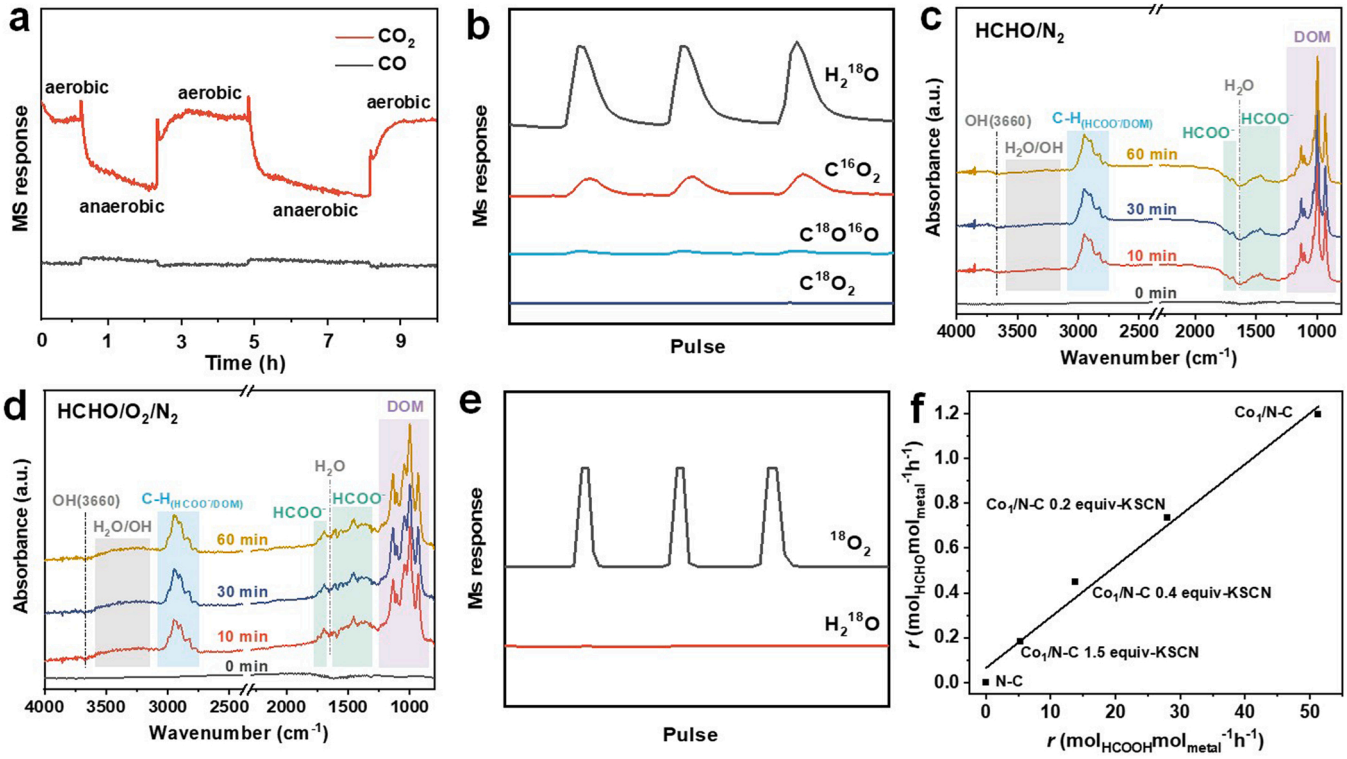

Fig. 4. (a) Evolution of concentrations of CO_2 (m/e=44) over Co_1/N-C under aerobic and anaerobic conditions. Reaction conditions: room temperature, GHSV of 12,000 mL·g_{cat}^{-1}·h^{-1}, 150 ppm HCHO, RH ~50%, 20% O_2/He balance for aerobic conditions and He balance for anaerobic conditions. (b) HCHO oxidation products were recorded by mass in the $^{18}O_2$ pulse-reaction experiment. In situ HCHO-DRIFTS of the Co_1/N-C as a function of time in a flow of HCHO/N_2 (c) and HCHO/O_2/N_2 (d). Reaction conditions: GHSV of 12,000 mL·g_{cat}^{-1}·h^{-1}, 150 ppm HCHO, RH ~50%, N_2 or 20% O_2 with N_2 balance, room temperature. (e) $^{18}O_2$ pulse reaction over Co_1/N-C in the absence of HCHO. (f) The HCHO oxidation rates as a function of the formic acid decomposition rates over Co_1/N-C with different KSCN treatments.

conditions and much higher under aerobic conditions, which suggested that the HCHO was eliminated by the complete oxidation to CO_2. In addition, no CO was found in the presence of oxygen coexistence, indicating that the selectivity of HCHO for CO_2 was ~99%. Many detailed studies [2,36–39] have clarified that the HCHO was catalytically decomposed near room temperature via two steps: first, the HCHO was transformed into formate intermediate with the help of surface hydroxyls, which was very fast with a very low energy barrier [2,39,40]; second, the decomposition of the formate intermediates (the rate-limiting step) involved two competing routes: i) carbon monoxide route ($HCOO_{ads} \rightarrow CO + H_2O \rightarrow CO_2 + H_2O$); ii) direct oxidation route ($HCOO_{ads} + [O]_s \rightarrow CO_2 + H_2O$, $[O]_s$ is the surface oxygen) [7,39].

To elucidate the reaction pathway of HCHO oxidation catalyzed by Co_1/N-C, ^{18}O isotope pulse reaction experiments were performed. As shown in Fig. 4b, introducing $^{18}O_2$ pulse as oxidant produced strong signal attributed to $H_2^{18}O$ as oxidation products, while the carbon dioxide was mainly $C^{16}O_2$ and trace CO_2 with ^{18}O labeled atoms ($C^{16}O^{18}O$ or $C^{18}O_2$, $C^{16}O_2$ / ($C^{16}O^{18}O$+$C^{18}O_2$) > 10) was observed. Based on these results obtained, the HCHO adsorption step was speculated as the hydroxyl-assisted path since the CO_2 was produced from the decomposing of the formate intermediates and the O atoms incorporated into HCHO were mainly from the water/hydroxyls rather than the molecular oxygen in the gas phase. As shown in Fig. 4c-d, significant DOM (860–1250 cm^{-1}) [2] and $HCOO^-$ (1290–1621 cm^{-1} and 1695 cm^{-1}) [2,41] species could be detected both on the Co_1/N-C surface under an N_2 and 20% O_2 atmosphere. This indicated that hydroxyl groups on the support surface facilitated DOM/$HCOO^-$ intermediate formation and that this process could occur without O_2 involvement (the HCHO adsorption step followed a hydroxyl-assisted path). Moreover, the -OH peak (Fig. S12, 3660 cm^{-1}) [2,41] on the catalyst surface at ~100% RH was significantly stronger than that at ~50% RH, which indicated that -OH on the catalyst surface could be regenerated by H_2O vapor in the gas stream [42–44]. The importance of water moisture was verified by controlled experiments performed at decreased humidity conditions (Fig. S13). When the RH was increased from 25% to 50%, the HCHO removal efficiency remained above 90% (Fig. S13), indicating that Co_1/N-C is well tolerated to water vapor. However, the catalytic activities measured at ~ 5% RH was much lower than that measured at ~ 25% RH. For the formate intermediates decomposing, the carbon monoxide route was not likely to happen because the oxidation of CO will lead to significant amount of $C^{16}O^{18}O$. Furthermore, we found the Co_1/N-C was inactive for CO catalytic oxidation even at 120 °C (Fig. S14), further confirming the infeasibility of the CO route. The possibility that the $H_2^{18}O$ was formed due to the exchange of oxygen atoms in water/surface hydroxyls with molecular $^{18}O_2$ was ruled out, according to the disappearance of $H_2^{18}O$ signal in the controlled experiment under the same condition without the introduction of HCHO (Fig. 4e). The direct oxidation pathway was preferred based on the evidence that only a small fraction of ^{18}O-labeled CO_2 and the immediate observation of $H_2^{18}O$ from the oxidation of formate intermediates.

In addition, over our Co_1/N-C catalysts with different KSCN treatments, the catalytic activity for HCHO oxidation was positively correlated with the formic acid decomposition ability, which implied that the single Co sites were responsible for decomposing formate intermediates and thus realizing the HCHO complete oxidation (Fig. 4f). Based on the above experimental results, we preliminarily proposed the reaction mechanism for HCHO complete oxidation over Co_1/N-C SACs. Adsorption of HCHO on the catalyst surface was achieved with the assistance of surface hydroxyls, leading to the formate intermediate coordinated to the Co-N_4 structure. The rate-determining step of the complete HCHO oxidation was the formate intermediate decomposing. This step occurs via the direct oxidation of formate intermediate into CO_2 and H_2O in the presence of gaseous oxygen. The compensated surface hydroxyls may be regenerated from the water moisture by the N-doped carbon under the

reaction atmosphere [42–44].

To further verify the oxidation mechanism of HCHO on Co_1/N-C, DFT calculations were performed. As shown in Fig. 5, -OH on the Co_1/N-C surface was regenerated by H_2O vapor in the gas stream (I→II). The HCHO adsorbed on the catalyst surface and reacted with surface OH to form H_2COOH* . The DFT calculation showed that this step had a small energy barrier of 0.16 eV (II→III). The formed H_2COOH* deprotonated generating H_2COO* , and this deprotonation step is slightly exothermic (III→IV, −0.38 eV). Formate (HCOO*) was then formed via the C−H bond breaking of H_2COO* with an activation barrier of 0.55 eV (IV→TS1→V). Next, oxygen molecules (O_2 *) were physically adsorbed onto the Co_1 site. O_2 * reacted with HCOO* to form OOH* species and CO_2 * (V→VII). This process needed to overcome an energy barrier of 0.75 eV (VI→TS2), indicating that this step (formate decomposition) was the kinetic rate-determining step, which was consistent with our experimental results of KSCN treatments. In addition, the energy barrier for the decomposition of formate intermediates by Co_1/N-C (0.75 eV) was lower than that reported in the references for noble metal Pt SACs (~1.12 eV) [2], which demonstrated that the highly dispersed CoN_x structure facilitated the decomposition of formate intermediates. Finally, gaseous CO_2 was released (VII→VIII) and OOH* decomposed to form gaseous H_2O with the assistance of proton (VIII→I) with a small activation barrier of 0.15 eV (VIII→TS3). Therefore, the HCHO removal by Co_1/N-C involved HCHO gradually forming formate under the action of hydroxyl on the catalyst surface (the hydroxyl on the catalyst surface could be compensated by H_2O vapor in the stream). Further, with the participation of O_2, formate decomposed to produce CO_2 and H_2O, where the O element in O_2 participated in the formation of H_2O.

4. Conclusions

In summary, we develop a versatile precursor-atomization strategy, and the synthesized Co_1/N-C exhibits unprecedented activity and excellent stability in formaldehyde abatement at room temperature, compared with the reported non-noble metal catalysts. The highly dispersed CoN_x active sites favor formate intermediate decomposition (the rate-limiting step for HCHO oxidation) and the low HCHO oxidation energy barrier are responsible for the excellent catalytic performance of Co_1/N-C for HCHO oxidation. Considering the low cost of elemental cobalt and the simpleness of our SACs synthesis approach, this work provides a practical and cost-effective pathway for widespread HCHO emission reduction.

Declaration of Competing Interest

The authors declare that they have no known competing financial interests or personal relationships that could have appeared to influence the work reported in this paper.

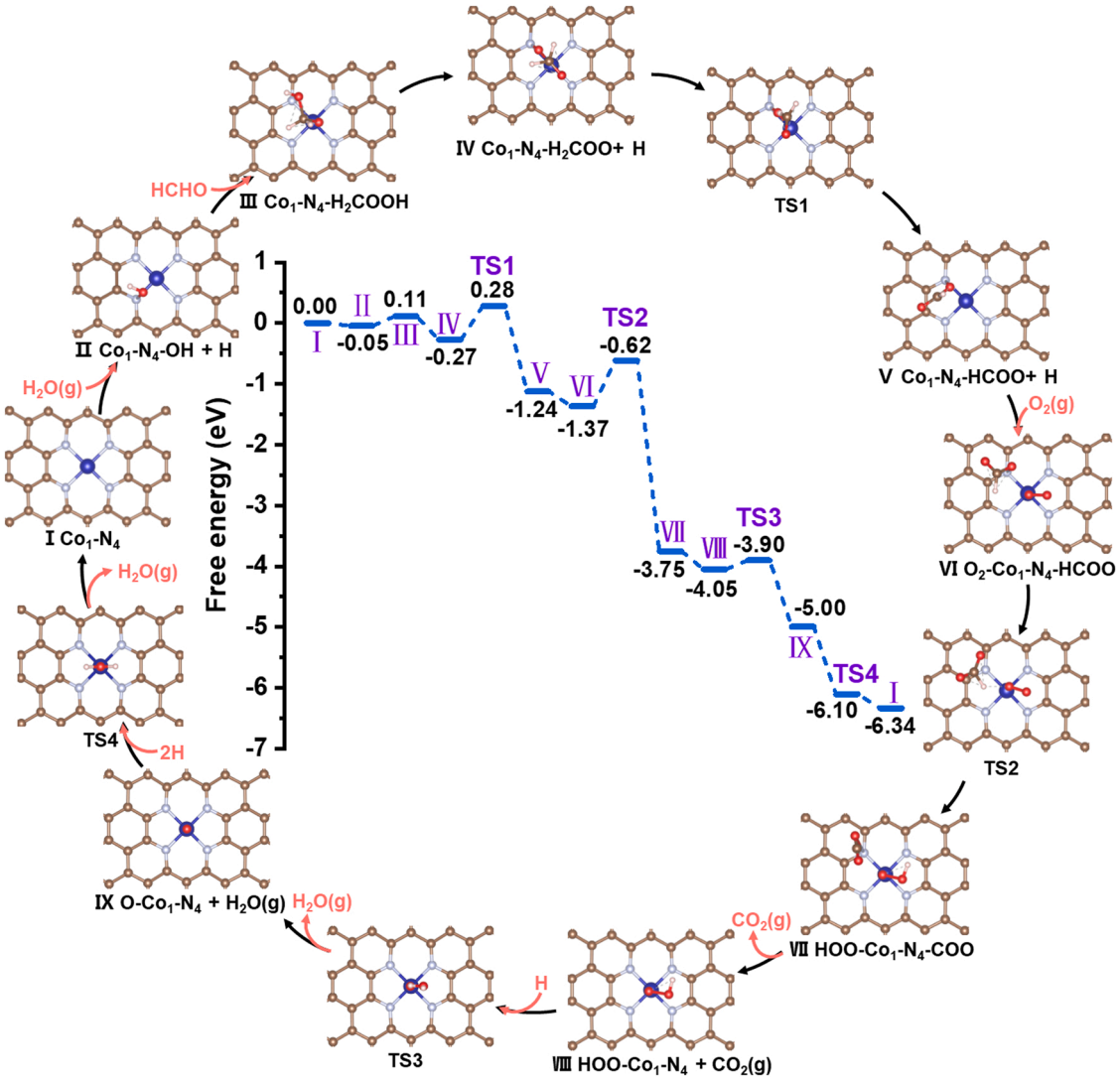

Fig. 5. Energy profiles and key elementary step intermediates structure of HCHO oxidation on Co_1/N-C.

Data Availability

Data will be made available on request.

Acknowledgments

This work was supported by the National Key Research and Development Program Nanotechnology Specific Project (No. 2020YFA0210900), the Science and Technology Key Project of Guangdong Province, China (2020B010188002), Guangdong Natural Science Funds for Distinguished Young Scholar (2022B1515020035), Guangdong Provincial Key R&D Programme (2019B110206002), the National Natural Science Foundation of China (22078371, 21938001, 21961160741, 22108315, U22A20428), Local Innovative and Research Teams Project of Guangdong Pearl River Talents Program (2017BT01C102), the Chemistry and Chemical Engineering Guangdong Laboratory (Grant No. 1922010). The authors thank eceshi (www.eceshi.com) for XPS analysis and ceshigo (www.ceshigo.com) for AC HAADF-STEM.

CRediT authorship contribution statement

X.H. and H.Z. developed the concept, designed these experiments, and wrote the paper. H.Z., G.G., Z.W., and Q.H. contributed to catalytic experiments and analyzed experimental data. X.H. and H.J. directed the project. All authors discussed the results and commented on the manuscript.

Appendix A. Supporting information

Supplementary data associated with this article can be found in the online version at doi:10.1016/j.apcatb.2023.122774.

References

[1] V.J. Cogliano, Y. Grosse, R.A. Baan, K. Straif, M.B. Secretan, F. El Ghissassi, V, Meeting report: summary of IARC monographs on formaldehyde, 2-butoxyethanol, and 1-tert-butoxy-2-propanol, Environ. Health Perspect. 113 (2005) 1205–1208.
[2] L. Zhang, Q. Bao, B. Zhang, Y. Zhang, S. Wan, S. Wang, J. Lin, H. Xiong, D. Mei, Y. Wang, Distinct role of surface hydroxyls in single-atom Pt_1/CeO_2 catalyst for room-temperature formaldehyde oxidation: acid-base versus redox, JACS Au 2 (2022) 1651–1660.
[3] T. Salthammer, S. Mentese, R. Marutzky, Formaldehyde in the indoor environment, Chem. Rev. 110 (2010) 2536–2572.
[4] C.J. Na, M.J. Yoo, D.C.W. Tsang, H.W. Kim, K.H. Kim, High-performance materials for effective sorptive removal of formaldehyde in air, J. Hazard. Mater. 366 (2019) 452–465.
[5] X. Zhu, C. Jin, X.-S. Li, J.-L. Liu, Z.-G. Sun, C. Shi, X. Li, A.-M. Zhu, Photocatalytic formaldehyde oxidation over plasmonic Au/TiO_2 under visible light: moisture indispensability and light enhancement, ACS Catal. 7 (2017) 6514–6524.
[6] X. Zhu, X. Gao, R. Qin, Y. Zeng, R. Qu, C. Zheng, X. Tu, Plasma-catalytic removal of formaldehyde over Cu–Ce catalysts in a dielectric barrier discharge reactor, Appl. Catal. B Environ. 170 (2015) 293–300.
[7] D. Zhu, Y. Huang, J.-j Cao, S.C. Lee, M. Chen, Z. Shen, Cobalt nanoparticles encapsulated in porous nitrogen-doped carbon: oxygen activation and efficient catalytic removal of formaldehyde at room temperature, Appl. Catal. B Environ. 258 (2019), 117981.
[8] A. Yusuf, C. Snape, J. He, H. Xu, C. Liu, M. Zhao, G.Z. Chen, B. Tang, C. Wang, J. Wang, S.N. Behera, Advances on transition metal oxides catalysts for formaldehyde oxidation: A review, Cat. Rev. 59 (2017) 189–233.
[9] T. Yang, Y. Huo, Y. Liu, Z. Rui, H. Ji, Efficient formaldehyde oxidation over nickel hydroxide promoted $Pt/\gamma\text{-}Al_2O_3$ with a low Pt content, Appl. Catal. B Environ. 200 (2017) 543–551.
[10] J. Guo, C. Lin, C. Jiang, P. Zhang, Review on noble metal-based catalysts for formaldehyde oxidation at room temperature, Appl. Surf. Sci. 475 (2019) 237–255.
[11] X. Sun, J. Lin, H. Guan, L. Li, L. Sun, Y. Wang, S. Miao, Y. Su, X. Wang, Complete oxidation of formaldehyde over TiO_2 supported subnanometer Rh catalyst at ambient temperature, Appl. Catal. B Environ. 226 (2018) 575–584.
[12] C. Ma, D. Wang, W. Xue, B. Dou, H. Wang, Z. Hao, Investigation of formaldehyde oxidation over $Co_3O_4\text{-}CeO_2$ and $Au/Co_3O_4\text{-}CeO_2$ catalysts at room temperature: effective removal and determination of reaction mechanism, Environ. Sci. Technol. 45 (2011) 3628–3634.
[13] Y. Huang, Y. Liu, W. Wang, M. Chen, H. Li, S.-c Lee, W. Ho, T. Huang, J. Cao, , Oxygen vacancy–engineered $\delta\text{-}MnO_x$/activated carbon for room-temperature catalytic oxidation of formaldehyde, Appl. Catal. B Environ. 278 (2020), 119294.
[14] Y. Huang, W. Fan, B. Long, H. Li, W. Qiu, F. Zhao, Y. Tong, H. Ji, Alkali-modified non-precious metal 3D-$NiCo_2O_4$ nanosheets for efficient formaldehyde oxidation at low temperature, J. Mater. Chem. A 4 (2016) 3648–3654.
[15] G. Busca, J. Lamotte, J.C. Lavalley, V. Lorenzelli, FT-IR study of the adsorption and transformation of formaldehyde on oxide surfaces, J. Am. Chem. Soc. 109 (2002) 5197–5202.
[16] Z. Han, C. Wang, X. Zou, T. Chen, S. Dong, Y. Zhao, J. Xie, H. Liu, Diatomite-supported birnessite–type MnO_2 catalytic oxidation of formaldehyde: preparation, performance and mechanism, Appl. Surf. Sci. 502 (2020), 144201.
[17] H. Wu, S. Ma, W. Song, E.J.M. Hensen, Density functional theory study of the mechanism of formaldehyde oxidation on Mn-doped ceria, J. Phys. Chem. C. 120 (2016) 13071–13077.
[18] A.Q. Wang, J. Li, T. Zhang, Heterogeneous single-atom catalysis, Nat. Rev. Chem. 2 (2018) 65–81.
[19] Y. Zhao, K.R. Yang, Z. Wang, X. Yan, S. Cao, Y. Ye, Q. Dong, X. Zhang, J.E. Thorne, L. Jin, K.L. Materna, A. Trimpalis, H. Bai, S.C. Fakra, X. Zhong, P. Wang, X. Pan, J. Guo, M. Flytzani-Stephanopoulos, G.W. Brudvig, V.S. Batista, D. Wang, Stable iridium dinuclear heterogeneous catalysts supported on metal-oxide substrate for solar water oxidation, Proc. Natl. Acad. Sci. U. S. A. 115 (2018) 2902–2907.
[20] M.J. Islam, M. Granollers Mesa, A. Osatiashtiani, J.C. Manayil, M.A. Isaacs, M. J. Taylor, S. Tsatsos, G. Kyriakou, PdCu single atom alloys supported on alumina for the selective hydrogenation of furfural, Appl. Catal. B Environ. 299 (2021), 120652.
[21] M.D. Marcinkowski, M.T. Darby, J. Liu, J.M. Wimble, F.R. Lucci, S. Lee, A. Michaelides, M. Flytzani-Stephanopoulos, M. Stamatakis, E.C.H. Sykes, Pt/Cu single-atom alloys as coke-resistant catalysts for efficient C–H activation, Nat. Chem. 10 (2018) 325–332.
[22] J. Ge, D. Zhang, Y. Qin, T. Dou, M. Jiang, F. Zhang, X. Lei, Dual-metallic single Ru and Ni atoms decoration of MoS_2 for high-efficiency hydrogen production, Appl. Catal. B Environ. 298 (2021), 120557.
[23] Z. Chen, E. Vorobyeva, S. Mitchell, E. Fako, M.A. Ortuño, N. López, S.M. Collins, P. A. Midgley, S. Richard, G. Vilé, J. Pérez-Ramírez, A heterogeneous single-atom palladium catalyst surpassing homogeneous systems for Suzuki coupling, Nat. Nanotechnol. 13 (2018) 702–707.
[24] S. Cao, M. Yang, A.O. Elnabawy, A. Trimpalis, S. Li, C. Wang, F. Goltl, Z. Chen, J. Liu, J. Shan, M. Li, T. Haas, K.W. Chapman, S. Lee, L.F. Allard, M. Mavrikakis, M. Flytzani-Stephanopoulos, Single-atom gold oxo-clusters prepared in alkaline solutions catalyse the heterogeneous methanol self-coupling reactions, Nat. Chem. 11 (2019) 1098–1105.
[25] X. Guo, G. Fang, G. Li, H. Ma, H. Fan, L. Yu, C. Ma, X. Wu, D. Deng, M. Wei, D. Tan, R. Si, S. Zhang, J. Li, L. Sun, Z. Tang, X. Pan, X. Bao, Direct, nonoxidative conversion of methane to ethylene, aromatics, and hydrogen, Science 344 (2014) 616–619.
[26] H. Zou, W. Rong, S. Wei, Y. Ji, L. Duan, H. Zou, W. Rong, S. Wei, Y. Ji, L. Duan, Regulating kinetics and thermodynamics of electrochemical nitrogen reduction with metal single-atom catalysts in a pressurized electrolyser, Proc. Natl. Acad. Sci. U. S. A. 117 (2020) 29462–29468.
[27] E. Zhang, L. Tao, J. An, J. Zhang, L. Meng, X. Zheng, Y. Wang, N. Li, S. Du, J. Zhang, D. Wang, Y. Li, Engineering the local atomic environments of Indium single-atom catalysts for efficient electrochemical production of hydrogen peroxide, Angew. Chem. Int. Ed. 61 (2022), e202117347.
[28] J. Sun, H. Xue, L. Lu, M. Gao, N. Guo, T. Song, H. Dong, J. Zhang, L. Wu, Q. Wang, Atomic-level modulation of local coordination environment at Fe single-atom sites for enhanced oxygen reduction, Appl. Catal. B Environ. 313 (2022), 121429.
[29] C. Wang, X. Hu, X. Hu, X. Liu, Q. Guan, R. Hao, Y. Liu, W. Li, Typical transition metal single-atom catalysts with a metal-pyridine N structure for efficient CO_2 electroreduction, Appl. Catal. B Environ. 296 (2021), 120331.
[30] C. Tang, A.E. Surkus, F. Chen, M.M. Pohl, G. Agostini, M. Schneider, H. Junge, M. Beller, A stable nanocobalt catalyst with highly dispersed CoN_x active sites for the selective dehydrogenation of formic acid, Angew. Chem. Int. Ed. 56 (2017) 16616–16620.
[31] C. Wang, H. Xie, S. Chen, B. Ge, D. Liu, C. Wu, W. Xu, W. Chu, G. Babu, P. M. Ajayan, L. Song, Atomic cobalt covalently engineered interlayers for superior lithium-ion storage, Adv. Mater. 30 (2018) 1802525.
[32] S. Yuan, J. Zhang, L. Hu, J. Li, S. Li, Y. Gao, Q. Zhang, L. Gu, W. Yang, X. Feng, B. Wang, Decarboxylation-induced defects in MOF-derived single cobalt atom@ carbon electrocatalysts for efficient oxygen Reduction, Angew. Chem. Int. Ed. 133 (2021) 21853–21858.
[33] M. Jiang, F. Wang, F. Yang, H. He, J. Yang, W. Zhang, J. Luo, J. Zhang, C. Fu, Rationalization on high-loading iron and cobalt dual metal single atoms and mechanistic insight into the oxygen reduction reaction, Nano Energy 93 (2022), 106793.
[34] P. Wang, Y.Y. Ren, R.T. Wang, P. Zhang, M.J. Ding, C.X. Li, D.Y. Zhao, Z. Qian, Z. W. Zhang, L.Y. Zhang, L.W. Yin, Atomically dispersed cobalt catalyst anchored on nitrogen-doped carbon nanosheets for lithium-oxygen batteries, Nat. Commun. 11 (2020) 1576.
[35] H. Tang, J. Zhang, M. Huang, J. Zhang, Y. Zhou, G. Wang, R. Wang, J. Chen, Remarkable performance of atomically dispersed cobalt catalyst for catalytic removal of indoor formaldehyde, J. Colloid Interface Sci. 624 (2022) 527–536.
[36] B. Chen, X. Zhu, M. Crocker, Y. Wang, C. Shi, Complete oxidation of formaldehyde at ambient temperature over $\gamma\text{-}Al_2O_3$ supported Au catalyst, Catal. Commun. 42 (2013) 93–97.
[37] H. Chen, Z. Rui, X. Wang, H. Ji, Multifunctional Pt/ZSM-5 catalyst for complete oxidation of gaseous formaldehyde at ambient temperature, Catal. Today 258 (2015) 56–63.

[38] J. Deng, W. Song, L. Chen, L. Wang, M. Jing, Y. Ren, Z. Zhao, J. Liu, The effect of oxygen vacancies and water on HCHO catalytic oxidation over Co_3O_4 catalyst: A combination of density functional theory and microkinetic study, Chem. Eng. J. 355 (2019) 540–550.
[39] D. Chen, Z. Qu, Y. Sun, K. Gao, Y. Wang, Identification of reaction intermediates and mechanism responsible for highly active HCHO oxidation on Ag/MCM-41 catalysts, Appl. Catal. B Environ. 142 (2013) 838–848.
[40] E.A. Batista, T. Iwasita, Adsorbed intermediates of formaldehyde oxidation and their role in the reaction mechanism, Langmuir 22 (2006) 7912–7916.
[41] S. Peng, Y. Rao, Y. Huang, T. Li, R. Li, J.-j Cao, S. Lee, N-Coordinated Ir single atoms anchored on carbon octahedrons for catalytic oxidation of formaldehyde under ambient conditions, Catal. Sci. Technol. 12 (2022) 4001–4011.
[42] H.-Z. Wu, L.-M. Liu, S.-J. Zhao, The role of the defect on the adsorption and dissociation of water on graphitic carbon nitride, Appl. Surf. Sci. 358 (2015) 363–369.
[43] S. Tang, S. Zhang, Adsorption of epoxy and hydroxyl groups on zigzag graphene nanoribbons: Insights from density functional calculations, Chem. Phys. 392 (2012) 33–45.
[44] C. Zhang, F. Liu, Y. Zhai, H. Ariga, N. Yi, Y. Liu, K. Asakura, M. Flytzani-Stephanopoulos, H. He, Alkali-metal-promoted Pt/TiO_2 opens a more efficient pathway to formaldehyde oxidation at ambient temperatures, Angew. Chem. Int. Ed. 51 (2012) 9628–9632.